Lunar atmospheric tidal effects in the plasma drifts observed by the Low-Latitude Ionospheric Sensor Network

Vince Eccles,[1] Donald D. Rice,[1] Jan J. Sojka,[1] Cesar E. Valladares,[2] Terence Bullett,[3] and Jorge L. Chau[4]

Received 11 November 2010; revised 9 April 2011; accepted 18 April 2011; published 21 July 2011.

[1] Data from the Low-Latitude Ionospheric Sensor Network are used to examine ionospheric electrodynamics during quiet, low solar conditions from September to November 2009. The ground-based magnetometers and the Jicamarca Vertical Incidence Pulsed Ionospheric Radar ionosonde in the Peruvian Sector are used to identify the neutral winds and plasma drifts that control the large-scale plasma structure of the ionosphere. It is observed that the solar- and lunar-driven semidiurnal tides have a significant influence on the background electrodynamics during this period of extreme solar minimum. The lunar tidal influence of the ionosphere electrodynamics is a large component of the variation of the vertical drift during the geophysically quiet study period. A significant portion, though not all, of the variation through the lunar month can be attributed to the lunar semidiurnal tide.

Citation: Eccles, V., D. D. Rice, J. J. Sojka, C. E. Valladares, T. Bullett, and J. L. Chau (2011), Lunar atmospheric tidal effects in the plasma drifts observed by the Low-Latitude Ionospheric Sensor Network, *J. Geophys. Res.*, *116*, A07309, doi:10.1029/2010JA016282.

1. Introduction

[2] The *E* region tidal neutral atmosphere motion and *F* region neutral winds drive ionospheric currents and generate electric fields in the ionosphere. The ground-based magnetometers measure the magnetic field deviations created by the Solar Quiet (SQ) current system as well as the equatorial electrojet (EEJ) currents in the ionosphere. The EEJ at the Earth's magnetic dip equator has a strong zonal current during the daytime. The zonal current within the EEJ is directly related to the zonal electric field and the vertical plasma drift, which is a primary driver of the low-latitude ionosphere. The general physics of the electrodynamics interaction of the neutral atmosphere, the magnetic field, and the ionosphere is generally understood and global models are beginning to approach good representations of average conditions [*Richmond et al.*, 1976; *Fesen et al.*, 1991a, 1991b; *Haerendel and Eccles*, 1992; *Crain et al.*, 1993; *Eccles*, 1998; *Millward et al.*, 2001]. However, the weather variation of the upper atmosphere and ionosphere is still not well modeled or even well understood [*Forbes et al.*, 2000]. The large-scale structure of the low-latitude ionosphere depends in a large part on two parameters: vertical $\mathbf{E} \times \mathbf{B}$ plasma drift and the meridional neutral winds. Neither of the two parameters can be adequately represented by empirical models when studying intraseasonal variability.

[3] This paper identifies a portion of the day-to-day weather variability as a potentially well-modeled variability related to the lunar neutral tides. Lunar tides in the upper atmosphere have been indirectly observed in magnetometer data for a number of decades [*Chapman and Bartels*, 1940]. *Bartels and Johnston* [1940a, 1940b], *Tarpley and Balsley* [1972], and we use the magnetometer placed at the Huancayo Geomagnetic Observatory (HUA, −12.04N, −75.82E) in Peru, which is very nearly under the EEJ. The deviation in the horizontal component (ΔH) is associated with neutral wind driven currents in the ionosphere. Magnetometers under the EEJ measure large *H* deviations during daytime associated with the zonal electric field and the electrojet Cowling effect [*Richmond*, 1973]. Lunar tidal modulation of the neutral wind dynamo and ionospheric electric fields become evident in the equatorial *F* region [*Bernhardt et al.*, 1976]. The TIECGM model has been used to examine the lunar tides in the low-latitude electric fields [*Stening et al.*, 1999]. *Stening and Fejer* [2001] examine the vertical drift data from Jicamarca radar for evidence of lunar tides. They fit data to a solar diurnal tide, a solar semidiurnal tide, and a lunar semidiurnal tide. They determine the lunar tide phase and magnitude over several months of data for daytime and separately for nighttime. They find a 2 to 3 m/s amplitude of modulation in the vertical plasma drift due to the lunar tides.

[4] In this paper we combine the Huancayo magnetometer data, Jicamarca ionosonde data, and a model of the ionosphere electrodynamics to demonstrate the large modulation of the vertical plasma drift during the very low solar minimum period of 1 September to 31 October 2009. These data

[1]Space Environment Corporation, Providence, Utah, USA.
[2]Institute for Scientific Research, Boston College, Chestnut Hill, Massachusetts, USA.
[3]CIRES, University of Colorado at Boulder, Boulder, Colorado, USA.
[4]Radio Observatorio de Jicamarca, Instituto Geofisico del Peru, Lima, Peru.

0148-0227/11/2010JA016282

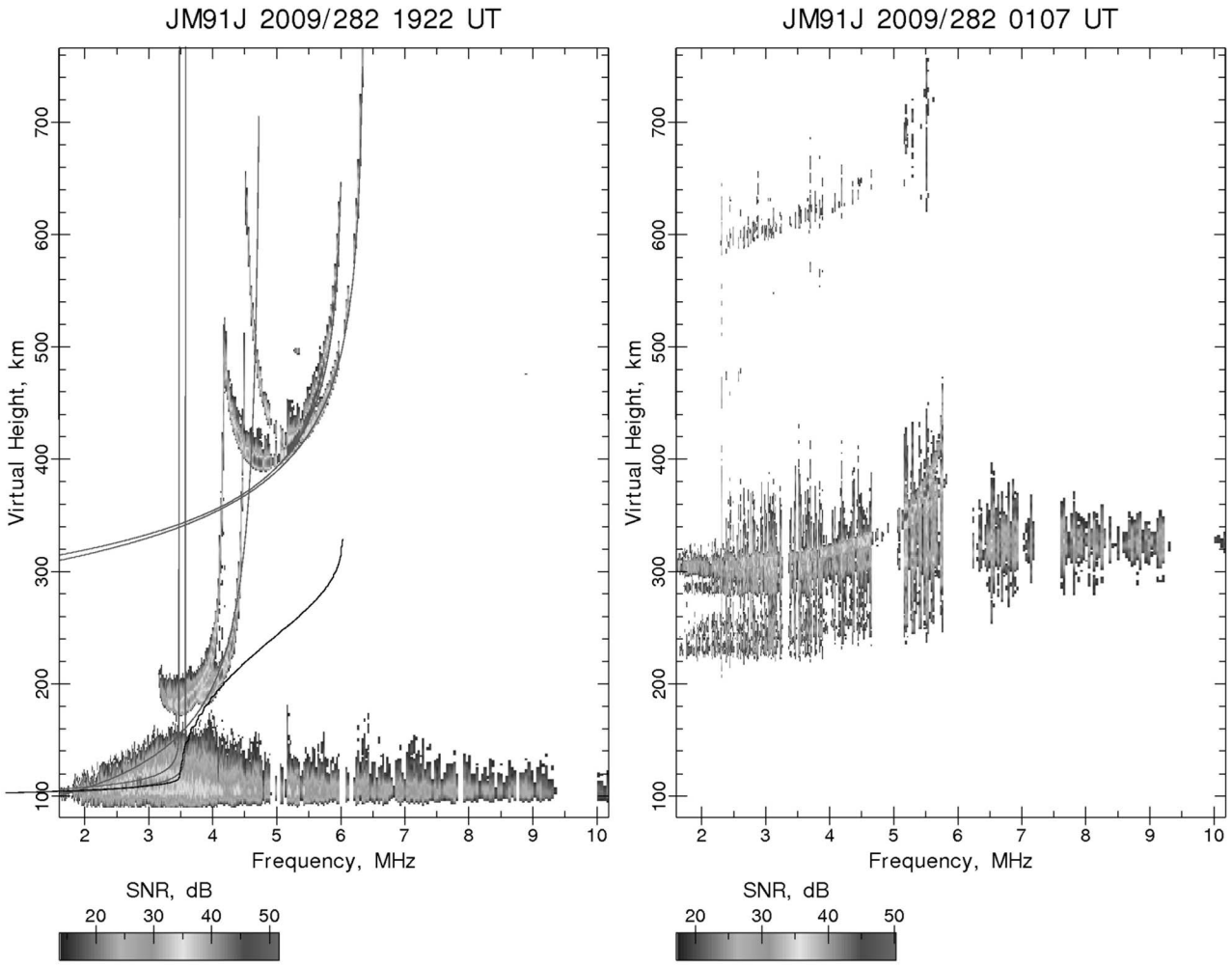

Figure 1. Two ionograms from the Jicamarca Vertical Incidence Pulsed Ionospheric Radar (VIPIR) analyzed by Expert System for Ionogram Reduction (ESIR): 9 October 2009 at (left) 19:22 UT and (right) 01:07 UT. For the 01:07 UT ionogram, ESIR finds no ionogram traces and provides no electron density profile.

are obtained as part of the Low-Latitude Ionospheric Sensor Network (LISN). We conclude that the lunar tidal influence is an important and predictable component of low-latitude ionosphere variability during low solar activity. The identification of a well-defined variation of the neutral wind field, zonal electric field, and vertical plasma drift related to lunar tides will provide better model drivers and reduce the unknown portions of the day-to-day weather in the low-latitude ionospheric drivers. Section 2 presents the ionosonde and magnetometer data from the Low-Latitude Ionospheric Sensor Network (LISN). Section 3 presents the models used to provide specifications of the low-latitude neutral winds, electrodynamics, and ionosphere structure with monthly average climatology comparisons. Section 4 examines the variability of the low-latitude system related to the lunar component of the neutral wind dynamo. Section 5 summarizes the paper.

2. LISN Observations

[5] The Low-Latitude Ionospheric Sensor Network (LISN) provides a multiple-point and multiple-instrument-type set of observations for the eventual definition of the low-latitude ionospheric weather in the South American Sector. For this paper, we examine the data from the Vertical Incidence Pulsed Ionospheric Radar (VIPIR) placed at the Jicamarca Radar Observatory (11.95°S, 76.87°W) and the ground-based magnetometer at the Huancayo Magnetic Observatory (12.04°S, 73.82°W). The time variation of the data from these two instruments has direct implications for the entire magnetic meridian because they represent observational insights into the electrodynamics of that meridian.

[6] The VIPIR instrument is a versatile HF instrument designed and manufactured by Scion Associates [*Grubb et al.*, 2008; *Bullett et al.*, 2010]. The LISN science team requested that the LISN VIPIR be operated in a manner that produced traditional ionogram observations of the ionosphere electron density profile. These ionograms have been analyzed with the Expert System for Ionogram Reduction (ESIR) software package developed by Space Environment Corporation [*Rice et al.*, 2009]. The ESIR analysis software is independent of the ionosonde hardware. ESIR uses a patented pattern recog-

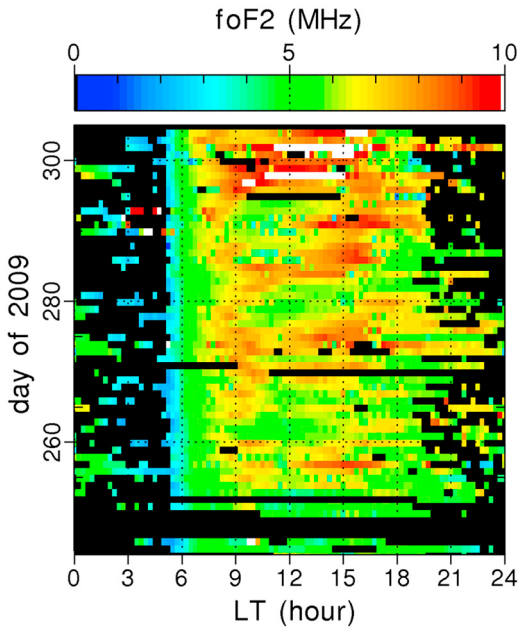

Figure 2. Peak frequency of the F_2 peak for each local time day from 1 September 2009 (day 244) to 1 November 2009 (day 305). The black regions represent either no data (days 247–249) or no f_oF_2 value obtained in the ESIR analysis.

nition technology [*Sojka et al.*, 2009] and an additional analysis step to ensure the robustness of the eventual electron profile and profile parameters. Figure 1 provides two ionograms from the Jicamarca VIPIR on 9 October 2009 at 19:22 UT and 01:07 UT. The ESIR software identified *E*, *F*1, and *F*2 layer traces in the ionogram of Figure 1 (left). A virtual height frequency profile is created; then the ESIR software uses the POLAN ionogram analysis program [*Titheridge*, 1985] to obtain a true height frequency profile (Figure 1, left, black line) and an electron density profile. The ionogram of Figure 1 (right) suffers from significant backscatter from irregularities in the *F* region ionosphere. The ESIR software analyzes this ionogram but determines that it cannot identify the ionosphere trace with certainty. The VIPIR data from 1 September to 31 October 2009 are the first test for the ESIR software for low-latitude ionosphere observations. Figure 2 presents the f_oF_2 values obtained from the automated ionogram analysis. The black space in the color plot represents periods of no data (mostly days 247–249) or periods where the ESIR software did not identify proper ionogram traces and hence no ionogram scaling was created. The daytime ionograms generally had clear traces and the f_oF_2 values are reliably obtained just prior to local sunrise at the Earth's surface. During the nighttime hours the ionograms suffered severe equatorial spread *F* (ESF) signatures, and often no ionogram trace could be found by the ESIR software. Even on visual inspection many of the nighttime ionograms had no definable F_2 trace. As seen in Figure 2, conditions made the nighttime ionograms difficult to analyze.

[7] The daytime f_oF_2 values through September and October 2009 of Figure 2 are modulated in regular patterns of increased and decreased f_oF_2. This modulation is most likely due to lunar semidiurnal atmospheric tidal effects on the zonal electric field (vertical plasma drift) as studied previously by *Bernhardt et al.* [1976] and *Stening and Fejer* [2001]. Higher values of upward vertical drift at local noon decreases the peak density (f_oF_2 value). The morning variation indicates that the morning rise in the vertical drift is strongly modulated by the lunar semidiurnal tide.

[8] We also present the *H* component from the magnetometer near Jicamarca at Huancayo Observatory near the magnetic dip equator in Figure 3. The magnetometer at Jicamarca shows similar results, but the data are not as clean as the Huancayo magnetometer. Figure 3 plots the horizontal component with the secular variation subtracted ($\Delta H = H - H_{SV}$) in the same format as Figure 2. The quiet day variation of the horizontal deflection is due mostly to the magnitude of the zonal EEJ current. The lunar variation in the EEJ current in the Peruvian Sector was also reported by *Tarpley and Balsley* [1972]. They identify seasonal variations in the lunar variations. We do not present a long enough period to investigate the seasonal differences. The strength of the noontime ΔH deflection varies approximately with a 14.75 day period associated with semidiurnal lunar tides. The EEJ zonal current is closely related to the zonal electric field and the $\mathbf{E} \times \mathbf{B}$ vertical plasma drift and, thus, related to the peak density of the ionosphere above the EEJ, and the equatorial electron density distribution of this meridian [*Rush and Richmond*, 1973].

[9] The noontime variations in the f_oF_2 values and ΔH are placed in line plots in Figure 4 for the 2 month period. The f_oF_2 and ΔH values plotted are averages of the hours near noon (10:00 LT to 13:00 LT). The lunar tide remains a coherent feature from mid-September through the end of October. The lunar modulation shows opposite correlation in these two observables as expected. Dashed sine curves with 14.75 day

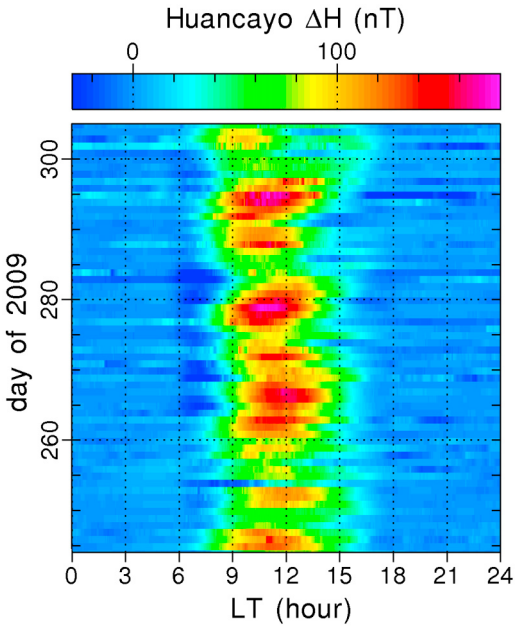

Figure 3. The magnitude of the quiet day variation of the horizontal component (ΔH) of the Huancayo Observatory magnetometer. The EEJ zonal current is closely related to the ΔH variation and the zonal electric field.

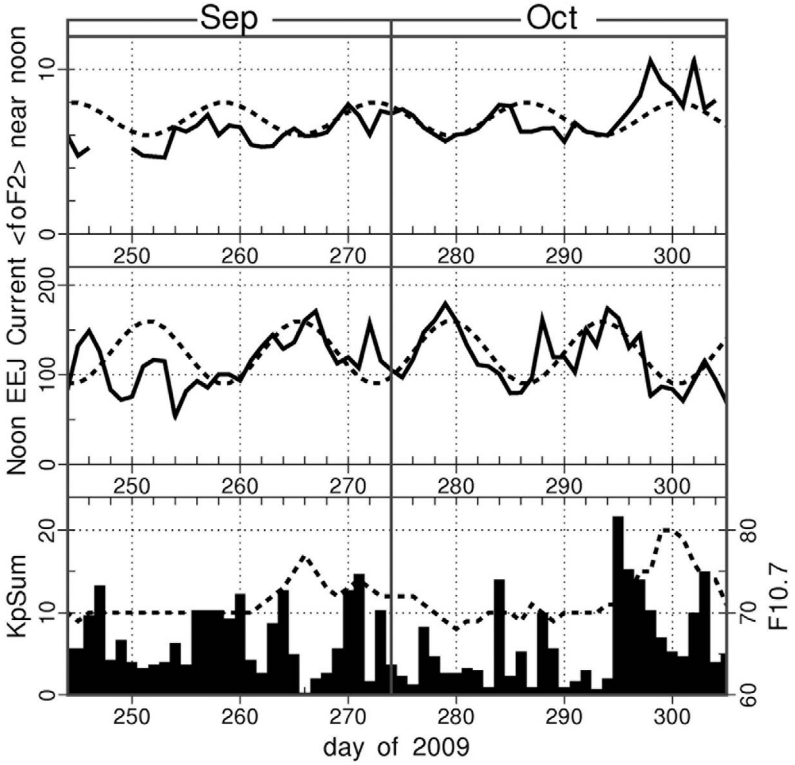

Figure 4. Noon analysis of VIPIR f_oF_2 and Huancayo ΔH values. (top) The noontime f_oF_2 variation (solid line) with a 14.75 day sine wave (dashed line). (middle) The noontime ΔH values (solid line) with a 14.75 day sine wave (dashed line). (bottom) The geophysical indices *KpSum* (histogram) and $F_{10.7}$ (dashed line).

periods and a 180° phase difference in Figure 4 (top and middle) are used to demonstrate the expected semidiurnal lunar tidal influence. The solar EUV and geomagnetic indices are also plotted to demonstrate that there is no correlation to solar or geomagnetic conditions. Both $F_{10.7}$ and *KpSum* indices are low during this period. Differences from the pure sinusoidal response of the ionosphere to the lunar influence perhaps indicate influences from tropospheric weather patterns and/or complex responses to high-latitude energy inputs.

3. Modeling the EEJ Current and *F* Region Response

[10] We combine ionospheric models of electric fields, electric currents, and electron densities to examine the self-consistent response of electrodynamics and the ionosphere to the lunar tide modulation of the solar-driven neutral wind field. The ionosphere model used is the Low-Latitude Ionosphere Sector (LLIONS) model. It is a direct descendent of the LowLat ionosphere model of *Anderson* [1981]. The LLIONS model solves for ionospheric ion (H^+, O^+, NO^+, O_2^+) and electron densities along dipole magnetic field lines in a single magnetic meridian. The dipole magnetic field lines are a best fit tilted-dipole definition to match the International Geomagnetic Reference Field Model (IGRF) at the dip equator in the longitude sector being modeled. The LLIONS model uses empirical models to set up the thermosphere, the vertical plasma drifts, and solar EUV drivers of the ionosphere. These include the MSIS-90 atmosphere [*Hedin*, 1991], the Horizontal Wind Model 2007 (HWM07) [*Drob et al.*, 2008], the Titheridge temperature model [*Titheridge*, 1998], the Scherliess-Fejer vertical plasma drift model [*Scherliess and Fejer*, 1999], and the ionization and absorption model of *Richards et al.* [1994a, 1994b]. For the day-to-day study of section 4, we have modified the LLIONS model to use a calculated vertical plasma drift rather than the Scherliess-Fejer model. The numerical solution of the ion and electron densities takes into account photochemistry and motion parallel and perpendicular to the magnetic field lines using rates and constants consistent with the USU ionosphere model [*Schunk and Sojka*, 1996].

[11] To compare the observed ΔH values of the Huancayo magnetometer with the modeled electric field and ionosphere conditions, we calculate zonal current contained in the EEJ using the EEJ model of *Haerendel and Eccles* [1992]. In the model, field line integrated conductivities and electrodynamics quantities are calculated using the ionosphere electron density and the thermosphere neutral density; then the zonal electric field in the model is used to calculate the current within the EEJ. For this initial climatological study we use the Scherliess-Fejer vertical plasma drift model to generate the zonal electric field ($\mathbf{E} \times \mathbf{B}$) to drive the EEJ region. This zonal EEJ current should be nearly proportional to a modeled ΔH. Figure 5 plots the 2 month average of the observed ΔH and a modeled ΔH component.

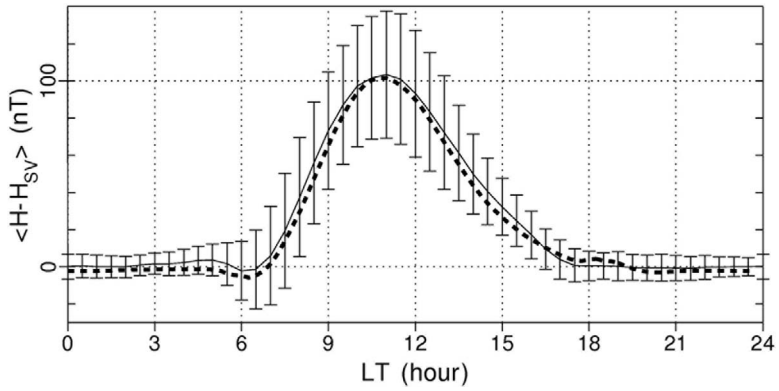

Figure 5. The average quiet day variation of H of the Huancayo Observatory magnetometer. The error bars indicate the standard deviation of the variation from the average value through the observation period. The dashed line plots the modeled deflection of H associated with the zonal EEJ current system.

In Figure 5, the zonal electric field is determined from the Scherliess-Fejer vertical drift model and the local value of the magnetic field. This climatological electric field generates a ΔH signature that is nearly identical to the average ΔH over the observations period. This demonstrates that a climatological monthly averaged electric field (vertical plasma drift) combined with climatologically driven ionosphere reproduces the monthly averaged EEJ current system.

[12] Figure 6 plots the average of the observed f_oF_2 for the 2 month period. The gray solid line again plots the modeled f_oF_2 for the ionosphere using the climatological drivers. There is a difference between the averaged observations and the climatological model result even though the EEJ comparison in Figure 5 was the same. The difference is best explained by the complicated relationship of the peak density to vertical plasma drifts at the dip equator whereas the magnetic deflection is proportional to the current in the EEJ which is linearly related to the zonal electric field times the conductance.

[13] We have compared the average of the daily ΔH values with the 2 month average ΔH values of Figure 5, and we observe that the average quiet day ΔH variation only occasionally matches any one of the individual days. For this period, the average trend does not represent any of the individual days. The variation through the 2 month period must be examined in a day-by-day analysis. Section 4 focuses on trying to identify the lunar tide associated with these observed day-to-day variations.

4. Modeling the Effect of the Lunar Tides

[14] We calculate the perpendicular electric fields using the Simple Electric Field (SEF) model of *Eccles* [1998] for the E × B motion within the LLIONS model for the Peruvian Sector. The SEF model uses the ionosphere electron densities of LLIONS, the neutral density of MSIS90, and the neutral

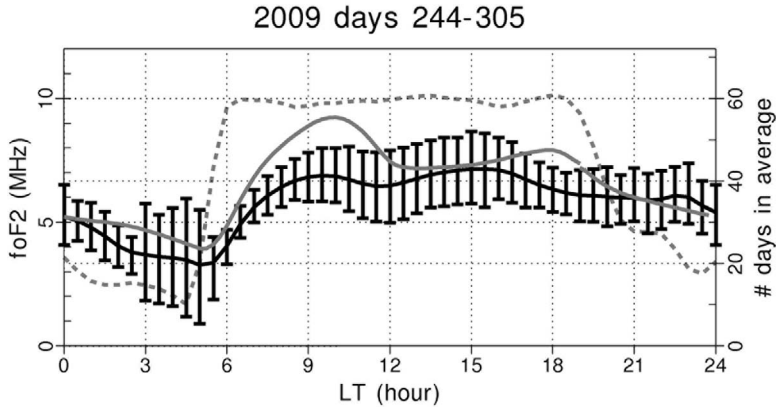

Figure 6. The average f_oF_2 values in local time over the observation period 1 September to 1 November 2009 (black line with error bars). Error bars represent the standard deviation of the weather variation through the month. The solid gray line is the climatological calculation of the f_oF_2 using *Scherliess and Fejer* [1999] vertical plasma drifts. The dashed gray line plots the number of days used for the average value.

Table 1. *E* Region Tides in Model

Tide	Hough Mode	A (m/s)	ϕ (h)	λ (km)
Solar diurnal	(1, −2)	130	20	∞
Solar semidiurnal	(2, 2)	65	05	83
Lunar semidiurnal	(2, 2)	65	23	83

wind field used within LLIONS to calculate the field line integrated electrodynamics quantities, which are combined to calculate directly the vertical and zonal electric fields and the resulting $\mathbf{E} \times \mathbf{B}$ plasma drifts [see *Eccles*, 1998]. The LLIONS ionosphere uses the calculated vertical drift at each 5 min time step to move the ionosphere solution forward 5 min in an explicit step. The thermospheric neutral wind field is generated for the *E* and *F* region altitudes ranges (100–150 km and 200–1000 km, respectively) using different models. The neutral winds in the *F* region altitudes (250 km up) were prescribed by the 2007 Horizontal Wind Model [*Drob et al.*, 2008]. The *E* region neutral winds (100–200 km) were prescribed by diurnal and semidiurnal tidal winds. The F_1 altitude range is a linear blend of the winds in these two ionosphere regions. For *F* region altitudes we have created a zonal wind pattern that reproduces the zonal drifts for Jicamarca at solar minimum reported by *Fejer et al.* [1985]. Additionally, we have found that the *F* region meridional winds in the low latitudes are essentially the same as the *E* region tidal meridional winds. This is understandable because only the zonal winds suffer from strong ion drag due to magnetic perpendicularity. For *E* region altitudes (150 km down) we use tidal modes in superposition. We include a solar diurnal mode (1,−2) (or (1,−1) in the work of *Tarpley* [1970a, 1970b]) and two semidiurnal modes (2,2), one solar and one lunar. Other tidal modes may be important, but we can approximately model the observations with these three tides. The solar diurnal tide is calculated by

$$u_S^{12} = A_S^{12} \sin\left(2\pi \frac{(t+\phi^{12})}{24}\right), \tag{1a}$$

$$u_E^{12} = A_E^{12} \sin\left(2\pi \frac{(t+\phi^{12})}{24} + \frac{\pi}{2}\right), \tag{1b}$$

where u_S and u_E are the southward and eastward winds, respectively, the As are the magnitudes of the (1,−2) Hough functions for the southward and eastward winds, t is the solar local time, and φ^{12} is the tidal phase for the solar (1,−2) mode. The solar semidiurnal tides are calculated by

$$u_S^{22} = A_S^{22} \sin\left(2\pi \frac{(2t+\phi^{22})}{24} + 2\pi \frac{z}{\lambda_{22}}\right), \tag{2a}$$

$$u_E^{22} = A_E^{22} \sin\left(2\pi \frac{(2t+\phi^{22})}{24} + 2\pi \frac{z}{\lambda_{22}} + \frac{\pi}{2}\right). \tag{2b}$$

The (2,2) mode changes phase with altitude with a wavelength defined by λ_{22}. The wavelength is approximately 85 km near the peak of conductivity in the *E* region. The lunar semidiurnal tide is calculated similarly, but a lunar age, ν, is incorporated into the formula, where lunar age indicates the hour difference of the moon from the current solar local time, t:

$$u_S^{L\,22} = A_S^{L\,22} \sin\left(2\pi \frac{(2t-2\nu+\phi^{L\,22})}{24} + 2\pi \frac{z}{\lambda_{22}}\right), \tag{3a}$$

$$u_E^{L\,22} = A_E^{L\,22} \sin\left(2\pi \frac{(2t-2\nu+\phi^{L\,22})}{24} + 2\pi \frac{z}{\lambda_{22}} + \frac{\pi}{2}\right). \tag{3b}$$

[15] We experimented with magnitudes and phases of the tides in our model using the following constraints. First, we assumed that the two semidiurnal tides, solar and lunar, are similar in magnitude as they arise primarily from similar forcings of gravitational and ocean surface modulation [*Chapman and Lindzen*, 1970; *Sawada*, 1965]. Second, the magnitude and phase of the solar diurnal tide and both semidiurnal tides are held constant through the 2 month period. These three tides will superimpose constructively and destructively through the lunar month. The best fit specifications of these three tides was determined using many model runs and comparing model calculations with observations of the magnetometer and peak density at local noon (Figure 4). Table 1 lists the best specifications for these three tides. The magnitude of the solar diurnal tide is 130 m/s, about 1/2 of its magnitude during solar maximum, and the phase angle is set at 20:00 LT. The solar and lunar semidiurnal tide magnitudes are 65 m/s. The altitude wavelength, λ, varies with the atmosphere thermal structure. At the Pederson conductivity peak (z = 125 km) for the (2,2) mode, we assume λ = 84 km [*Tarpley*, 1970a]. The results using the Simple Electric Field (SEF) model and the LLIONS ionosphere model for the 2 month period using the above wind and tides definitions are shown in Figure 7 (left). Figure 7 (right) presents the LLIONS results using the *Scherliess and Fejer* [1999] vertical drift model. The LLIONS/SEF model results have the same character in magnitudes and variations of ΔH and f_oF_2 observations (Figures 2 and 3). Including the lunar tide effect with solar-driven winds in electrodynamics modulates the otherwise very static seasonal trends when using only solar tides. The inclusion of lunar tides provides a calculable space weather variation of the low-latitude ionosphere.

[16] *Stening and Fejer* [2001] reported 2 to 3 m/s lunar tide effects in the vertical plasma drift during solar medium conditions. This modeling study during solar minimum produces a 7 m/s lunar tide modulation at noon supporting earlier modeling studies that semidiurnal tides are more prominent during solar minimum conditions [*Fesen et al.*, 1991b]. Indeed, *Tarpley* [1970a] used a lunar semidiurnal tide amplitude of 7.5 m/s to model observed lunar modulation of Solar Quiet current patterns during solar medium conditions.

[17] *Fesen et al.* [1991b] also demonstrates a *Kp* influence of the semidiurnal tides in phase and magnitude, though the influence is weaker at lower latitudes. Deviations between the model and the observations may demonstrate some correlation with elevated *Kp* (Figure 4), but the correlation is weak.

5. Conclusion

[18] The first analysis of the LISN VIPIR observations revealed a clear 14.75 day modulation in the F_2 peak (f_oF_2). The same 14.75 day modulation is also apparent in the

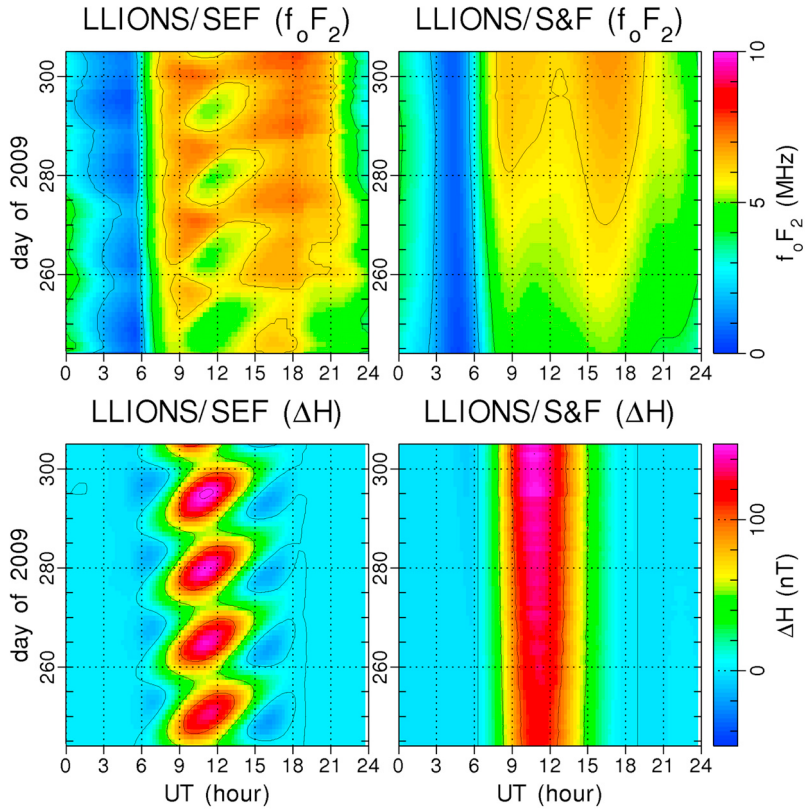

Figure 7. Model results using (left) the Low-Latitude Ionosphere Sector (LLIONS) model and the Simple Electric Field model and (right) LLIONS and the *Scherliess and Fejer* [1999] vertical drift model. Plots of (top) f_oF_2 and (bottom) ΔH of the EEJ.

Huancayo magnetometer observations under the EEJ. We proposed the obvious, that the modulation is driven by a lunar semidiurnal tide. We modeled the low-latitude ionosphere of the Peruvian Sector using a physics-based ionosphere model, tidal neutral wind modes, low-latitude electric field calculation, and an EEJ current model to demonstrated that the lunar and solar semidiurnal tides dominate the daily magnitude of the zonal electric field, which drives the zonal EEJ current and the *F* region vertical plasma drift. The lunar tide accounted for a significant portion of the day-to-day variability that is not described by the Scherliess and Fejer plasma drift model, which provides excellent average drifts but no lunar component.

[19] The day-to-day variability in both the ΔH and f_oF_2 observations was modeled by LLIONS using a revised neutral wind model consisting of six terms describing tides (see equations (1)–(3)). The coefficients of these tidal modes for the Jicamarca meridian are summarized in Table 1. These amplitudes are different from prior studies, both theoretical and observational. This we attribute to the extremely low solar minimum conditions and the extended magnetically quiet period of the September–October 2009 study interval.

[20] The solar diurnal tidal mode, which is driven by solar energy deposition, was present in the data but its magnitude was reduced during this period of extreme solar minimum in comparison to periods of higher solar activity. An important conclusion of this study is that a climatological model of the equatorial vertical plasma drift (zonal electric field) can reasonably include a lunar tidal component during geomagnetically quiet periods. Including the lunar effects in the vertical drift magnitude will reduce the variance between the model and the observed ionosphere. The variability of the f_oF_2 and ΔH observations not described by the simple description of the solar and lunar tides appears to have some relationship with days of elevated *Kp* though there may be tropospheric phenomena driven modulations as well. Carefully identifying the solar and lunar tides will help identify the remaining drivers of low-latitude ionospheric weather.

[21] **Acknowledgments.** This study was funded under NSF grant ATM0745714 to Space Environment Corporation and a subcontract to Space Environment Corporation from Boston College under NSF grant ATM0521487. The authors thank the support of the LISN Engineering Team at Instituto Geofisico del Peru and, in particular, C. de la Jara, who helped in the installation operation and data processing of the VIPIR system.

[22] Robert Lysak thanks the reviewers for their assistance in evaluating this paper.

References

Anderson, D. N. (1981), Modeling the ambient, low latitude *F* region ionosphere: A review, *J. Atmos. Terr. Phys.*, *43*, 753–762, doi:10.1016/0021-9169(81)90051-9.

Bartels, J., and H. F. Johnston (1940a), Geomagnetic tides in horizontal intensity at Huancayo, 1, *J. Geophys. Res.*, *45*, 269–308.

Bartels, J., and H. F. Johnston (1940b), Geomagnetic tides in horizontal intensity at Huancayo, 2, *J. Geophys. Res.*, *45*, 485–512.

Bernhardt, P. A., D. A. Antoniadis, and A. V. da Rosa (1976), Lunar perturbation in columnar electron content and their interpretation in terms of

dynamo electrostatic fields, *J. Geophys. Res.*, *81*, 5957–5963, doi:10.1029/JA081i034p05957.
Bullett, T., A. Malagnini, M. Pezzopane, and C. Scotto (2010), Application of Autoscala to ionograms recorded by the VIPIR ionosonde, *Adv. Space Res.*, *45*, 1156–1172, doi:10.1016/j.asr.2010.01.024.
Chapman, S., and J. Bartels (1940), *Geomagnetism*, Oxford Univ. Press, London.
Chapman, S., and R. S. Lindzen (1970), *Atmospheric Tides: Thermal and Gravitational*, D. Reidel, Dordrecht, Netherlands.
Crain, D., R. Heelis, and G. Bailey (1993), Effects of electrical coupling on equatorial ionospheric plasma motions: When is the *F* region a dominant driver in the low-latitude dynamo?, *J. Geophys. Res.*, *98*, 6033–6037, doi:10.1029/92JA02195.
Drob, D. P., et al. (2008), An empirical model of the Earth's horizontal wind fields: HWM07, *J. Geophys. Res.*, *113*, A12304, doi:10.1029/2008JA013668.
Eccles, J. V. (1998), A simple model of low-latitude electric fields, *J. Geophys. Res.*, *103*, 26,699–26,708, doi:10.1029/98JA02657.
Fejer, B., E. Kudeki, and D. Farley (1985), Equatorial *F* region zonal plasma drifts, *J. Geophys. Res.*, *90*, 12,249–12,255, doi:10.1029/JA090iA12p12249.
Fesen, C., R. Roble, and E. Ridley (1991a), Thermospheric tides at equinox: Simulations with coupled composition and auroral forcings: 1. Diurnal component, *J. Geophys. Res.*, *96*, 3647–3661, doi:10.1029/90JA02188.
Fesen, C., R. Roble, and E. Ridley (1991b), Thermospheric tides at equinox: Simulations with coupled composition and auroral forcings: 2. Semidiurnal component, *J. Geophys. Res.*, *96*, 3663–3677, doi:10.1029/90JA02189.
Forbes, J. M., S. E. Palo, and X. Zhang (2000), Variability of the ionosphere, *J. Atmos. Sol. Terr. Phys.*, *62*, 685–693, doi:10.1016/S1364-6826(00)00029-8.
Grubb, R. N., R. Livingston, and T. W. Bullett (2008), A new general purpose high performance HF radar, paper presented at 2008 General Assembly, Union Radio Sci. Int., Chicago, Ill.
Haerendel, G., and J. V. Eccles (1992), The role of the equatorial electrojet in the evening ionosphere, *J. Geophys. Res.*, *97*, 1181–1192, doi:10.1029/91JA02227.
Hedin, A. E. (1991), Extension of the MSIS thermosphere model into the middle and lower atmosphere, *J. Geophys. Res.*, *96*, 1159–1172, doi:10.1029/90JA02125.
Millward, G., I. Müller-Wodar, A. Aylward, T. Fuller-Rowell, A. Richmond, and R. Moffett (2001), An investigation into the influence of tidal forcing on *F* region equatorial vertical ion drift using a global ionosphere-thermosphere model with coupled electrodynamics, *J. Geophys. Res.*, *106*, 24,733–24,744, doi:10.1029/2000JA000342.
Rice, D. D., J. J. Sojka, and D. C. Thompson (2009), An Expert System for Ionosonde Reduction (ESIR), paper presented at CEDAR Workshop, Natl. Sci. Found., Santa Fe, N. M., June.
Richards, P. G., J. A. Fennelly, and D. G. Torr (1994a), EUVAC: A solar EUV flux model for aeronomic calculations, *J. Geophys. Res.*, *99*, 8981–8992, doi:10.1029/94JA00518.
Richards, P. G., J. A. Fennelly, and D. G. Torr (1994b), Correction to "EUVAC: A solar EUV flux model for aeronomic calculations," *J. Geophys. Res.*, *99*, 13,283–13,284, doi:10.1029/94JA01446.
Richmond, A. D. (1973), Equatorial electrojet, I. Development of a model including winds and instabilities, *J. Atmos. Terr. Phys.*, *35*, 1083–1103, doi:10.1016/0021-9169(73)90007-X.
Richmond, A. D., S. Matsushita, and J. D. Tarpley (1976), On the production mechanism of electric currents and fields in the ionosphere, *J. Geophys. Res.*, *81*, 547–555, doi:10.1029/JA081i004p00547.
Rush, C. M., and A. D. Richmond (1973), The relationship between the structure of the equatorial anomaly and the strength of the equatorial electrojet, *J. Atmos. Terr. Phys.*, *35*, 1171–1180, doi:10.1016/0021-9169(73)90013-5.
Sawada, R. (1965), The possible effect of oceans on the atmospheric lunar tide, *J. Atmos. Sci.*, *22*, 636–643, doi:10.1175/1520-0469(1965)022<0636:TPEOOO>2.0.CO;2.
Scherliess, L., and B. G. Fejer (1999), Radar and satellite global equatorial *F* region vertical drift model, *J. Geophys. Res.*, *104*, 6829–6842, doi:10.1029/1999JA900025.
Schunk, R. W., and J. J. Sojka (1996), USU model of the global ionosphere, in *Solar-Terrestrial Energy Program: Handbook of Ionospheric Models*, edited by R. W. Schunk, pp. 153–172, Cent. for Atmos. and Space Sci., Logan, Utah.
Sojka, J. J., D. C. Thompson, and D. D. Rice (2009), Sounding transformation and recognition, Patent 7,541,967, U.S. Patent and Trademark Off., Washington, D. C.
Stening, R. J., and B. G. Fejer (2001), Lunar tide in the equatorial *F* region vertical ion drift velocity, *J. Geophys. Res.*, *106*, 221–226, doi:10.1029/2000JA000175.
Stening, R. J., A. D. Richmond, and R. G. Roble (1999), Lunar tides in the Thermosphere-Ionosphere-Electrodynamics General Circulation Model, *J. Geophys. Res.*, *104*, 1–13, doi:10.1029/98JA02663.
Tarpley, J. D. (1970a), The ionospheric wind dynamo: I. Lunar tides, *Planet. Space Sci.*, *18*, 1075–1090, doi:10.1016/0032-0633(70)90109-1.
Tarpley, J. D. (1970b), The ionospheric wind dynamo: II. Solar tides, *Planet. Space Sci.*, *18*, 1091–1103, doi:10.1016/0032-0633(70)90110-8.
Tarpley, J. D., and B. B. Balsley (1972), Lunar variations in the Peruvian electrojet, *J. Geophys. Res.*, *77*, 1951–1960, doi:10.1029/JA077i010p01951.
Titheridge, J. E. (1985), UAG-93: Ionogram analysis with the generalized program POLAN, http://www.ngdc.noaa.gov/stp/solar/uaglist.html, World Data Cent. for Sol.-Terr. Phys., Boulder, Colo.
Titheridge, J. E. (1998), Temperatures in the upper ionosphere and plasmasphere, *J. Geophys. Res.*, *103*, 2261–2277, doi:10.1029/97JA03031.

T. Bullett, CIRES, University of Colorado at Boulder, Boulder, CO 80309, USA.
J. L. Chau, Radio Observatorio de Jicamarca, Instituto Geofisico del Peru, Lima 33, Peru.
V. Eccles, D. D. Rice, and J. J. Sojka, Space Environment Corporation, 221 N. Gateway Dr., Ste. A, Providence, UT 84332, USA. (vince.eccles@spacenv.com)
C. E. Valladares, Institute for Scientific Research, Boston College, Chestnut Hill, MA 02467, USA.